Bollhorst, T. and Jakob, S. and Köser, J. and Maas, M. and Rezwan, K.

Chitosan supraparticles with fluorescent silica nanoparticle shells and nanodiamond-loaded cores

Chitosan supraparticles with fluorescent silica nanoparticle shells and nanodiamond-loaded cores†

T. Bollhorst,[a] S. Jakob,[a] J. Köser,[b] M. Maas*[a] and K. Rezwan[a]

Spherical colloidal structures with a sparsely or densely packed shell of nanoparticles have been the subject of intense research efforts for more than a decade. Research has focused on the utilization of aqueous, soft, or solid cores mainly on the micron-scale. A synthesis route that combines a stabilizing biopolymer core in combination with small (15 nm) or ultrasmall (5 nm) nanoparticles templated on the surface is still missing and pivotal to push these structures further into bionanotechnological applications. Here, we present core–shell supraparticles with a nanodiamond-loaded chitosan core and a shell assembled from fluorescent silica nanoparticles with controlled packing density which feature final sizes significantly below one micrometer. The synthesis route is highly versatile and represents a general approach for the synthesis of sophisticated supraparticles with shells formed from distinct nanoparticle shells and biopolymer cores loaded with selective nanoparticles.

Introduction

Supraparticles, *i.e.* hierarchically self-assembled structures formed from colloidal building blocks, with a core–shell architecture comprising a surface of functional nanoparticles and a hard, soft or gas-filled interior have garnered research interest in a wide range of fields, like drug delivery,[1] bioimaging,[2] catalysis,[3] energy storage,[4] or photonics.[5] Various synthesis routes exist for the creation of such colloidal structures, including the directed assembly of colloidal clusters,[6,7] the mechanical stabilization of Pickering-emulsions,[8,9] the amphiphilicity-driven formation of nanoparticle vesicles from polymer-grafted colloids[10,11] or the surface templating of nanoparticles against colloidal substrates.[12,13] Each of these synthesis routes has certain advantages and drawbacks, as described in our recent review.[14]

Specifically, utilizing the latter of the aforementioned synthesis routes allows for a favourable control of the size, monodispersity, and other architectural properties of such structures. For instance, the synthesis of the substrate particles can be precisely controlled on the nano-scale ahead of the templating step. Additionally, the packing density and arrangement of the nanoparticles in the shell may be tuned to create a distinct pore network between the

interstitial spacing of the shell-forming particles.[15] Furthermore, if a polymer is chosen as the matrix of the core material it can feature stabilizing and encapsulating capacities, which is potentially advantageous in comparison to a liquid core. Also, by utilizing specific functional colloids for the synthesis process (*i.e.* plasmonic, superparamagnetic, or fluorescent nanoparticles) the final structures can be designed to feature distinct physical properties for bionanotechnology applications.[16] Here, small[17,18] or ultrasmall[19] inorganic nanoparticles are of increasing interest for the synthesis of the shell, as they are rapidly moving into the central focus in the field of bio-nano science.[20–22]

However, the miniaturization of such structures towards sizes significantly below 1 μm with shells formed from (ultra-)small nanoparticles remains challenging. For instance, the synthesis of such structures based on the greatly utilized Pickering-emulsion route is problematic as small nanoparticles are more prone to momentum transfer from the solvent molecules and tend to detach from oil–water interfaces,[23] leading to a hampered formation of emulsion-based capsules on the nano-scale. Also, nano-sized emulsion droplets exhibit an increased Laplace pressure[1] and a higher tendency for Ostwald ripening which renders the emulsion instable without the use of specialized surfactants or polymers.[24,25] These obstacles for the synthesis of nano-scaled supraparticles with a shell formed from nanoparticles can be overcome if the particles are absorbed on a biopolymer-based colloidal template.

Various combinations of polymer-based core templates and distinct types of colloidal particles adsorbed on the core surface have been investigated in the past couple of years. Specifically, in numerous studies PNIPAm (poly *N*-isopropylacrylamide) – or

a PNIPAm derivative – was employed for the synthesis of the core material due to its unique thermoresponsive properties. Kim & Weitz et al. initially reported the adsorption of sulphate- or carboxylate-functionalized polystyrene particles with diameters between 20 nm and 4 μm on PNIPAm microgels.[26] Karg et al. templated gold colloids against different temperature and pH sensitive PNIPAm or PNIPAm derivative based nano-/microgel substrate particles, to control the optical properties of the resulting structures by tuning the plasmonic coupling properties.[27–29] Du et al. investigated the templating of silica nanoparticles against PNIPAm substrate particles and further studied a fusing of the shell.[30] Other particle-armored micron-sized supraparticles with a different polymer core material include structures with a PMMA,[31,32] wax,[33,34] or alginate[35] core. As mentioned above, a great number of nanoparticle-templated colloidal substrates aim at bionanotechnology applications. Hence, the utilization of a biopolymer core matrix, in contrast to potentially cytotoxic PNIPAm,[36] and (ultra-)small nanoparticles with distinct physical properties adsorbed on their surface, is of high interest. Additionally, the miniaturization to dimensions significantly below 1 μm is pivotal for the potential utilization of such core–shell supraparticles in the field of bio-nano science.

Following these considerations, the investigation of a bio-degradable polymer with little to no intrinsic toxicity,[37] for instance PLGA, polycaprolactone, or chitosan as the precursor for a nanometer-sized core material is of high interest. Particularly, chitosan, a polysaccharide copolymer consisting of varying amounts of β-(1→4)-linked 2-amino-2-deoxy-β-D-glucopyranose (GlcN) and 2-acetamido-2-deoxy-β-D-glucopyranose, has moved into the focus for the development of safe and efficient bio-medical products.[38] Chitosan and its derivatives have gained considerable research interest for their use as materials in bionanotechnology applications[39–41] and have been subject of recent reviews.[42,43] Chitosan nanoparticles are of specific interest for the synthesis of polyelectrolyte complexes,[44] for the oral delivery of macromolecules[45] or for the intravenous delivery of small interfering RNA (siRNA).[46] More specifically, low molecular weight chitosan with a fraction of acetylation (F_A) value (i.e. the percentage of acetyl groups to amine groups in the chitosan chain) of approx. 50%, was recently found to possess an advantageous degradation behaviour in vitro and in vivo.[47] Nanoparticles formed from this specific type of chitosan were previously investigated by Guo et al. and also showed favourable behaviour in in vitro drug delivery experiments.[48,49] Therefore, an improved understanding of the formation of nano-scaled supraparticles with a core formed from chitosan and templated with nano-particles with specific functionality is of high interest for the controlled synthesis of multivalent supraparticles.

Here we report a direct facile approach for the creation of such spherical core–shell structures with cores formed from low molecular weight chitosan which comprise a tailor-made sparely or densely templated surface of (ultra-)small fluorescent silica nanoparticles. Furthermore, we also investigated the system for the synthesis of nanodiamond-loaded chitosan cores combined with the surface templating of small fluorescent silica nanoparticles. This study provides one of the first reports of the combination of a biopolymer colloid templated with <20 nm inorganic nanoparticles with distinct physical properties. The formation of structures at this length-scale is particularly hard to predict as the additivity of attractive van der Waals, repulsive double layer, and solvation forces described by DLVO theory does not apply for nanoparticles below 20 nm.[50]

Experimental section

Materials and methods

Low molecular weight Chitosan (CS) was purchased from Bioneer A/S, Denmark. Tetraethyl orthosilicate (TEOS), tetraethyl ortho-silicate (TMOS), L-arginin, ethylenediaminetetraacetic acid (EDTA), glutaraldehyde solution 25% (GA), and rhodamine b isothio-cyanate mixed isomers (RBITC) were purchased from Sigma-Aldrich without further purification. Detonation diamond nanopowder (ND) was purchased from PlasmaChem GmbH, Germany.

Synthesis of RBITC-doped small SiO₂ nanoparticles (S-SiO₂-NP)

RBITC-doped small SiO_2 nanoparticles (S-SiO₂-NP) were synthesized by adjusting a previously published method by Shahabi and coworkers.[51] For the synthesis of a stock solution, 174 mg L-arginin was added to 169 mL DI water and stirred in a 500 mL round-flask for 30 min. Subsequently, 5 mL of a 0.5 mg mL⁻¹ RBITC aqueous solution were added to the flask. The mixture was heated to 70 °C, upon which 11.16 mL TEOS were added dropwise under vigorous stirring. After reacting for 24 h, the mixture was cooled to room temperature and transferred to a dialysis tube with a cut-off value of 12 kDa and then dialyzed against DI water for 6 days, changing the dialysis media once a day. The stock dispersion was finally stored at 4 °C.

Synthesis of ultrasmall RBITC-doped SiO₂ nanoparticles (US-SiO₂-NP)

RBITC-doped ultrasmall SiO_2 nanoparticles (US-SiO₂-NP) were synthesized based on a previously reported method by Ma et al.[52,53] Briefly, 2 mL of a 0.02 M ammonia aqueous solution were added into 17.5 mL DI water. Subsequently, 0.5 mL of a 0.5 mg mL⁻¹ RBITC aqueous solution was added to the flask. Following this, 127 μL TMOS were added dropwise and the mixture was stirred overnight. The mixture was subsequently heated to 80 °C and stirring was stopped. After reacting for 24 h, the mixture was cooled to room temperature and cleaned via dialysis as described above. The stock dispersion was finally stored at 4 °C.

Preparation of nanodiamond dispersions

Nanodiamond dispersions were prepared as described previously.[54] To produce negatively charged nanodiamonds, 1 g of powder was annealed for 5 h at 450 °C in air. For positively charged nanodiamonds, 1 g of powder was annealed for 5 h at 500 °C in a 1 bar hydrogen atmosphere. The treated powders were suspended in 100 mL Millipore water and ultrasonicated using a

high power disintegrator at 250 W for 3 h. Subsequently, the dispersions were centrifuged twice for 1 h at 16 000g. The obtained bluish brown dispersions exhibited nanodiamond concentrations of approx. 5 mg mL^{-1}.

Synthesis of native, SiO$_2$-NP surface-templated and combined nanodiamond-loaded and SiO$_2$-NP surface-templated chitosan particles

Native chitosan nanoparticles were synthesized in accordance to a previously described counterion-mediated and nonsolvent-aided method by Guo *et al.*[48,49] All reaction steps were performed at room temperature. For the synthesis of native chitosan particles, 5 mg of CS (see table in Fig. 2 for chitosan properties) was dissolved in 1 mL DI water at neutral pH and stirred for 30 min. Subsequently, the counter-ion complexation was performed for 30 min after the addition of 1 mg of EDTA. Upon subsequent addition of 0.75 mL ethanol, the precipitation of the chitosan was induced within the mixture which led to the formation of nanoparticles from the solution. This became evident in a change of the opalescence of the mixture. The particles were then cross-linked for 3 h *via* the addition of 3 μL of GA (GA might be replaced in future studies with genipin[55]). The dispersion was finally dialyzed for 3 days to remove the EDTA and excess GA. Dialysis was performed in Spectrum Labs Float-A-Lyzer tubes with a MW cut-off of 100 kDa. After the

dialysis process, approximately 1.5 mL of the upper volume of the supraparticle dispersion was transferred to a new vial for storage.

Chitosan supraparticles templated with SiO$_2$ nanoparticles were self-assembled as depicted in Fig. 1. Soft non-cross-linked colloidal chitosan templates are formed as described above. Approx. 5 min after the addition of EtOH, which induced the chitosan NP formation, respective silica NP dispersions were added to the *de novo* formed chitosan particles. Depending on the silica particle type and intended packing density, varying amounts of nanoparticles were added for the templating of the chitosan particles (*i.e.* 100 μL of a 10 mg mL^{-1} dispersion for a sparely or 100 μL of a 40 mg mL^{-1} dispersion for a densely packed surface of S-SiO$_2$-NP and 100 μL of a 3 mg mL^{-1} dispersion for the synthesis of a sparely packed surface of US-SiO$_2$-NP). After letting the particles adsorb on the surface for 15 min, 3 μL of GA solution was added to each sample dispersion and cross-linked for 3 h before transferring the samples to dialysis tubes. The dialysis process was performed as described for the native chitosan particles. The chitosan particles templated with the high concentration of S-SiO$_2$-NP showed the formation of a very thin sediment layer on the bottom of the dialysis tube at the end of the dialysis process, whilst the other samples showed no sediment formation. The bottom part of the dialyzed dispersions was left unperturbed
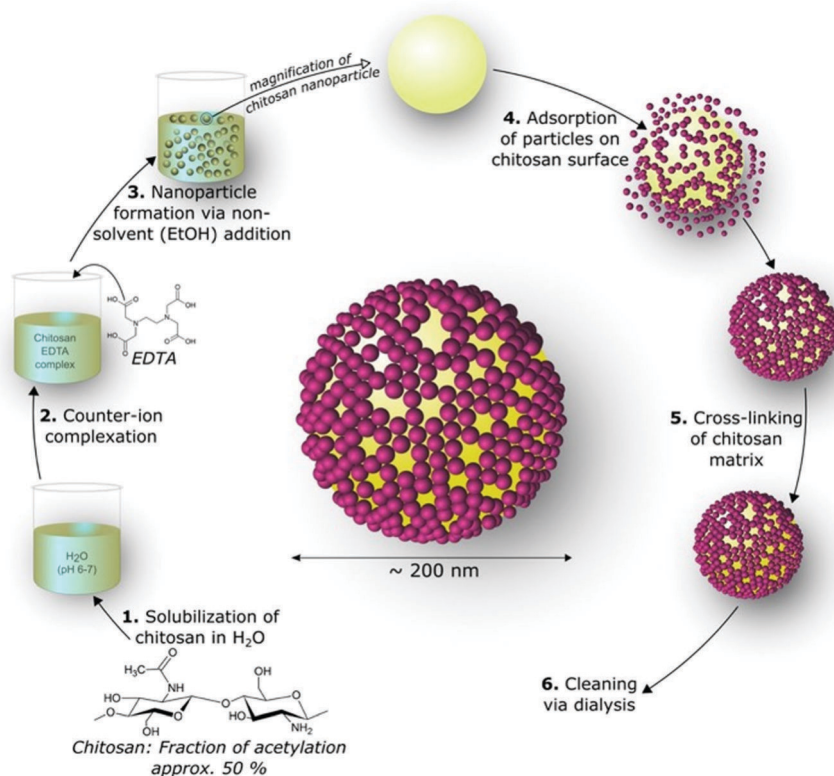
Fig. 1 Synthesis scheme of colloid templated chitosan particles: (1) solubilization of chitosan with an F_A value of approx. 50% in pH neutral (6–7) demineralized water; (2) counter-ion complexation of chitosan with EDTA; (3) addition of ethanol for reduction of chitosan solubility resulting in nucleation and nanoparticle formation; (4) schematic zoom-in on templating process of fluorescent nanoparticle on chitosan substrate; (5) cross-linking of chitosan matrix with glutaraldehyde; (6) dialysis against DI water to remove free EDTA and unreacted glutaraldehyde.

and approx. 1.5 mL of the upper volume of each dialyzed sample was transferred to a new vial for storage and characterization.

For the synthesis of nanodiamond-loaded and SiO_2 nano-particle templated chitosan particles, we added 10 μL of the nano-diamond stock dispersion with a concentration of 5 mg mL^{-1} prior to the addition of EtOH which induces the chitosan nanoparticle formation (see Fig. 6A for scheme of the synthesis route). This enabled the nanodiamonds to be encapsulated inside the chitosan particles. The rest of the synthesis was performed as described for the (U)S-SiO_2-NP templated chitosan supraparticles. The final supraparticle dispersion showed, similarly to the high concentration S-SiO_2-NP sample, the formation of a very thin sediment layer. This layer was again left unperturbed and approx. 1.5 mL of the upper volume of the dialyzed sample was transferred to a new vial for storage and characterization.

Characterization of supraparticles

Morphologies of the native nanoparticles and supraparticles were visualized with a Zeiss EM 900 at an acceleration voltage of 80 kV, respectively. Approx. 2 μL of the varying samples were deposited on TEM grids and dried overnight. Scanning electron microscopy (SEM) images were acquired using a Zeiss Supra40. A 10 μL droplet was deposited directly on silicon substrates and dried overnight. The samples did not require a sputter coating. DLS and ζ-potential measurements were performed with a Malvern Nano ZSP zetasizer without diluting the samples. For each DLS measurement, 1 mL of the sample dispersion was filled into disposable PMMA cuvettes. Measurements were performed in backscatter setup mode at 173°. For ζ-potential measurements, small aliquots of each dispersion were measured in disposable folded capillary cells. Fluorescence emission spectra (excitation at 550 nm) were recorded with a LS 50 Spectrometer (Perkin Elmer, Germany). Samples were measured in glass cuvettes.

Results and discussion

The utilized low molecular weight chitosan was thoroughly analysed in previous studies by Weinhold and coworkers. Here, the molecular weight was determined via size-exclusion chro-matography to be 10.3 kg mol^{-1} and the fraction of acetylation (F_A) was quantified by ^{1}H-NMR spectroscopy and determined to be 0.48.[56] It is worth mentioning that the F_A value plays a pivotal role on the solubility and was found to only render chitosan soluble at neutral pH if the value is very close to 50%.[57] For the counterion-mediated and nonsolvent-aided formation of nanoparticles, chitosan was dissolved at almost neutral pH which renders the molecule cationic due to the protonation of its amine groups. The complexation of the chitosan can therefore be easily achieved via the addition of EDTA, which upon its dissolution in water and partial dissocia-tion of its carboxyl groups functions as the anionic counterion. The subsequent addition of ethanol induced the precipitation of the chitosan–EDTA complex and resulted in the nucleation
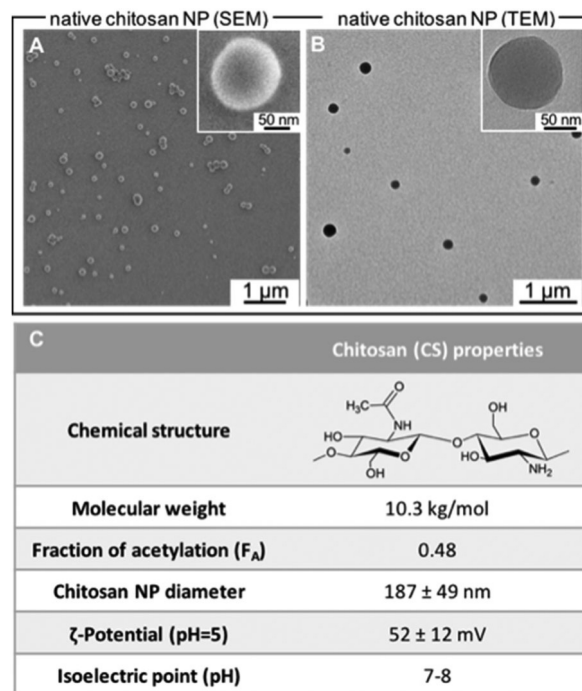

Fig. 2 (A) SEM and; (B) TEM micrographs of native chitosan particles (insets show close-up images of chitosan NPs) and; (C) properties of low molecular weight chitosan utilized for the particle synthesis and resulting colloidal properties.

and growth of nanoparticles. A crosslinking of the chitosan chains is then achieved via the addition of a small amount of a 25% glutaraldehyde solution. The EDTA and unreacted glutaraldehyde are subsequently removed via dialysis against DI water. The pH of the final chitosan nanoparticle dispersion was determined to be approx. 5. Fig. 2A and B show SEM and TEM micrographs of the prepared chitosan nanoparticles. DLS experiments indicated the diameters of the particles to be 187 ± 49 nm with a very low PDI of 0.05, rendering them ideal templates for the synthesis of supraparticles with a very narrow size distribution. This is a significant advantage over colloidal capsules formed via emulsion routes where high monodispersity can be achieved for micron-sized droplets, whilst nanodroplets, or more specifically nanoemulsions,[58] are usually prepared via extensive ultrasonication or with an ultraturrax, often leading to polydisperse droplet size distributions. Electrophoretic light scattering measurements further showed a ζ-potential of 52 ± 12 mV at pH 5–6 and the isoelectric point was found via titration measurements to be between pH 7–8. It should be noted that the utilization of this specific type of chitosan is pivotal for our templating route. Because the templating process is a distinct type of solution self-assembly,[59] that relays on electrostatic inter-actions of the larger chitosan template particles and the smaller silica nanoparticles, the utilization of ionic liquids[60] or shifting the pH to acidic values and using aqueous solutions of acetic acid or HCl,[61] which are usually used for the solubilization of chitosan with higher molecular weights and different acetylation patterns, would likely cause a loss of control over the successful surface templating step. Such destabilization and loss of control over the
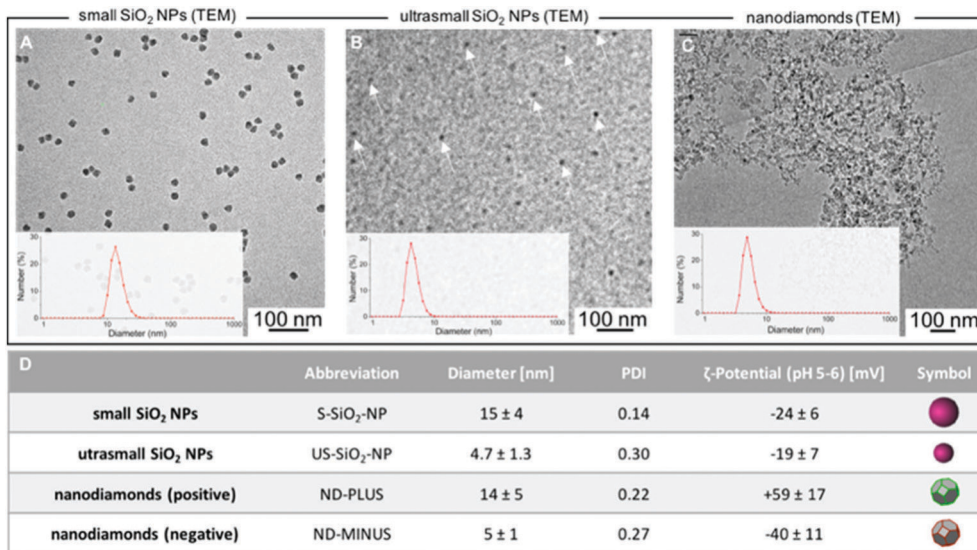
Fig. 3 TEM micrographs and list of properties of native inorganic nanoparticles utilized for the templating and/or loading of chitosan particles (insets show DLS number distribution results of the respective NPs). (A) Small fluorescent silica particles; (B) ultra-small fluorescent silica particles (some of the particles are provided with an arrow for their easier identification); (C) nanodiamonds.

assembly process might be caused by enhanced aggregation of the small particles inside the electrostatic cloud of the template particles.[62] Generally, besides their often utilized positive effects in the field of self-assembly, weak acids or bases, salts, surfactants or polyelectrolytes can also cause self-assembly processes to fail. For instance, we observed the successful formation of colloidal capsules (colloidosomes) on a Pickering emulsion route from thoroughly dialyzed dispersion, but failed to form capsules from an unwashed iron oxide nanoparticle dispersion containing residual salts.[63]

Inorganic nanoparticles prepared for the templating as well as for the loading process of the chitosan particles are depicted in Fig. 3. The small SiO_2 NP (S-SiO_2-NP) showed virtually no particle-to-particle fusing in the TEM (see Fig. 3A). Light scattering experiments revealed a diameter of 15 ± 4 nm as well as a low PDI of 0.14 and a ζ-potential of −24 ± 6 mV. In rudimentary cell experiments, the particles could be readily identified via fluorescent microscopy (Fig. S2, ESI†). Ultrasmall SiO_2 NP (US-SiO_2-NP) exhibited a diameter of 4.7 ± 1.7 nm and a ζ-potential of −19 ± 7 mV. However, in contrast to the S-SiO_2-NP, the PDI featured a higher value of 0.30. For easier identification, some of the US-SiO_2-NP were marked with an arrow in the TEM micrograph. The particles showed no apparent fusing in the TEM. Fluorescence spectra for both silica nanoparticle types are shown in Fig. S1 (ESI†). After their dispersion in pure DI water the positively (59 ± 17 mV) and negatively charged (−40 ± 11 mV) nanodiamonds showed diameters of 14 ± 5 nm and 5 ± 1 nm respectively. However, electron micrographs revealed a significant agglomeration of the particles on the TEM grids, which correlates to the higher PDI of 0.22 for the positively and 0.27 for the negatively charged nanodiamonds and accordingly explains the significant increase in size of the positive nanodiamonds in the DLS measurements.

The inorganic particles were subsequently diluted and used for the templating processes. To tailor the density and amount of S-SiO_2-NP adsorbed on the surface of the chitosan particles we investigated two different particle concentrations: a low concentration of 10 mg mL^{-1} and a high concentration of 40 mg mL^{-1}. As depicted in the synthesis scheme in Fig. 1, 100 μL of either the low or highly concentrated S-SiO_2-NP dispersion was slowly added to the chitosan nanoparticle dispersion prior to the cross-linking step. Fig. 4A.1–A.3 and B.1–B.3 show overview and close-up micrographs of the varying samples, clearly indicating an increase of adsorbed particles for the higher concentrated S-SiO_2-NP dispersion. The fusing of the supraparticles is attributed to drying effects on the TEM grids. We also observed a significant number of single/unfused supraparticles for both samples. In DLS measurements, the chitosan particles templated with a low concentration of S-SiO_2-NP exhibited a size of 203 ± 54 nm, in comparison to chitosan particle templated with a high concentration of S-SiO_2-NP of 228 ± 72 nm. However, a gradual decrease of the ζ-potential was observed for the templated chitosan particles in comparison to the native chitosan particles. We detected a change of the ζ-potential from the native chitosan particles from 52 ± 12 mV to 34 ± 6 mV for the low and 18 ± 5 mV for the high templating concentrations of S-SiO_2-NP (Fig. 4D). This serves as further evidence for the successful adsorption of the particles on the chitosan surface. The fluorescence properties of the S-SiO_2-NP were maintained after their templating against the chitosan substrate particles. However, the overall fluorescence intensity is mitigated, which is most likely caused either by partial absorption of the emitted light through the chitosan particles or by fluorescence proximity quenching, which is a result of energy transfer between directly neighbouring fluorescent particles.[64]

To study the further miniaturization of the system, we also investigated ultrasmall fluorescent silica nanoparticles for the
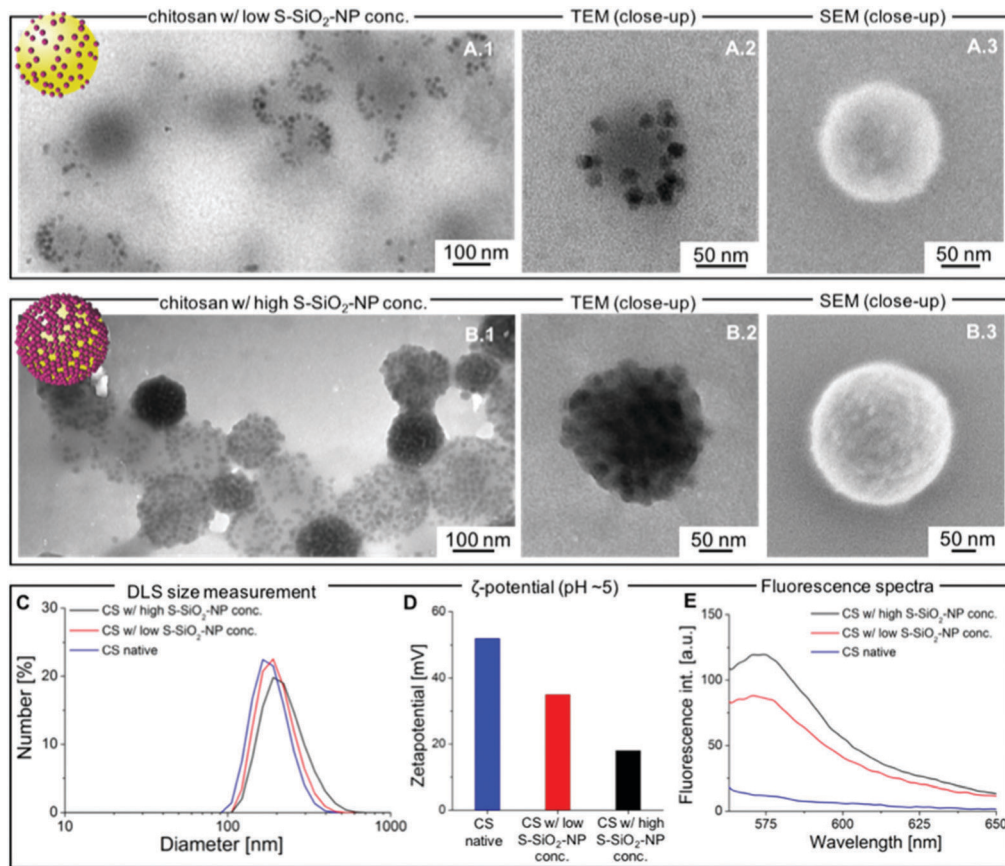
Fig. 4 Chitosan particles templated with varying amounts of fluorescent S-SiO$_2$-NP. TEM and SEM micrographs of chitosan templates (A) spare and (B) high surface coverage with S-SiO$_2$-NP (A.1 and B.1): the fusing of particles is attributed to drying effects on the TEM grids. (C) DLS measurement number distribution results and (D) zeta-potential results of the native chitosan particles and particles templated with low and high conc. of S-SiO$_2$-NP; (E) fluorescence spectra.

templating process. Different concentrations of US-SiO$_2$-NP were chosen for the templating process for which we all observed a successful adsorption on the chitosan templates. Fig. 5 shows TEM and SEM micrographs of templated chitosan particles. The close-up pictures reveal a sparse coverage of the chitosan particles when a total amount of 0.3 mg of US-SiO$_2$-NP was added. Due to the marginal difference of the material density of the silica and chitosan colloids as well as the small size of the silica particles, the resulting material contrast of the varying materials is very low in the TEM micrographs, impeding the visual analysis. However, the US-SiO$_2$-NP are still reasonably visible as very small black dots on the chitosan particle in Fig. 5A.2 and are also visible as blurry dots in the topography micrograph in Fig. 5A.3. We did not observe a significant change in size for the US-SiO$_2$-NP templated chitosan particles (see Fig. 5B). However, the adsorption of the US-SiO$_2$-NP is further evidenced in a substantial decrease of the ζ-potential from 52 $\pm$ 12 mV to 23 $\pm$ 5 mV. Due to the low concentration of the US-SiO$_2$-NP we were not able to measure a fluorescence signal. Unfortunately, increasing the concentration of US-SiO$_2$-NP for the templating process led to a high amount of free US-SiO$_2$-NP (see Fig. S3, ESI†).

To compare the templating process with another type of material class we also investigated the adsorption of nanodiamonds

on the chitosan particles. As noted above, the native nano-diamond dispersions showed significant signs of fusing and aggregation. This led to an unspecific adsorption and hetero-agglomeration with chitosan particles for the positively as well as the negatively charged nanodiamonds (see Fig. S4, ESI†). Hence, the utilization of well dispersed nanoparticles for the here described templating process is a prerequisite for a successful adsorption process for the prevention of flocculation and to finally preserve a stable colloidal dispersion.

We next studied the loading of the chitosan particles with inorganic nanoparticles and were able to incorporate nano-diamonds in the chitosan particles, which could potentially serve as a placeholder for pharmaceutical agents in future studies. The left part of the scheme in Fig. 6A shows the synthesis process for the loading of the chitosan particles. The nanodiamonds (50 μg) were added to the chitosan–EDTA complex prior to the precipitation of the chitosan via the addition of ethanol. Interestingly, while templating with nano-diamonds led to unspecific adsorption and agglomeration, loading within the chitosan core could be successfully achieved (see Fig. 6B and Fig. S5B.1, B.2, ESI†). In DLS measurements, the chitosan nanodiamond-loaded composite particles featured a size of 158 $\pm$ 45 nm. The ζ-potential was slightly decreased
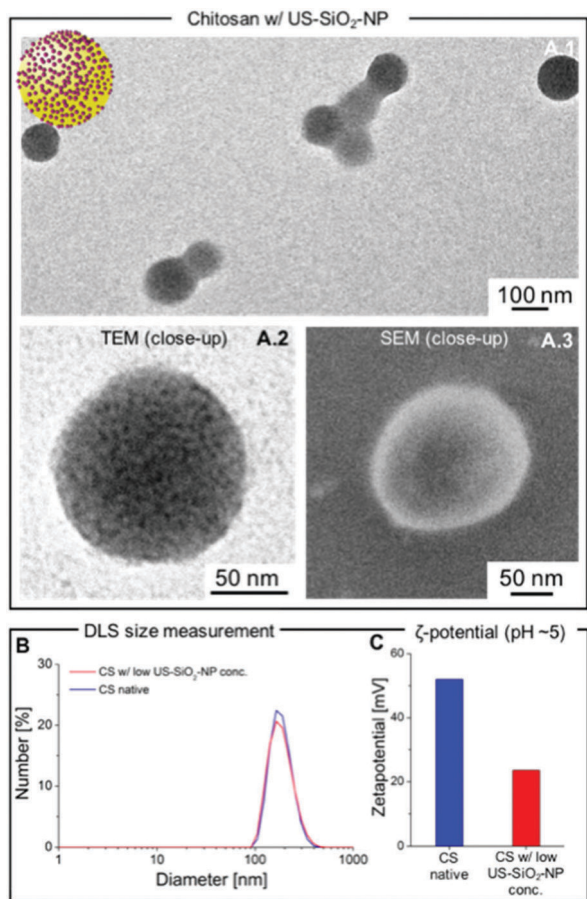
Fig. 5 Chitosan particles templated with US–SiO$_2$-NP; (A) electron micrographs of the resulting particles, showcasing a spare coverage of the chitosan templates with the US–SiO$_2$-NP. (B) No size increase was observed for the US–SiO$_2$-NP/chitosan composites, however, (C) the adsorption of the particles is clearly evidenced in a significant decrease of the zeta-potential.

Fig. 6 (A) Scheme for the synthesis of nanodiamond loaded and S–SiO$_2$-NP templated chitosan particles; TEM micrographs of two different samples of chitosan particles; (B) loaded with nanodiamonds and (C) loaded with nanodiamonds and templated with S–SiO$_2$-NP; (D) results of DLS measurements and (E) zeta-potential measurements for the templated particles.

(32 ± 5 mV) in comparison to the native chitosan particles. In future studies, the nanodiamonds or other colloids incorporated in the core (*e.g.* reduced graphene oxide[65]) could serve as vehicles for cytostatic agents or other pharmaceuticals, which is especially interesting for designing nanocarriers that feature a multi-stage release.[66] Subsequently to the loading of the core with nanodiamonds, we further templated the chitosan particles with 4 mg of S–SiO$_2$-NP. The synthesis is shown in the right part of Fig. 6A. We observed a substantial amount of nanodiamond-loaded and S–SiO$_2$-NP-surface-templated chitosan composite particles (see. Fig. 6C for a TEM micrograph). In DLS measurements we observed a size of 171 ± 49 nm for the ND-loaded and S–SiO$_2$-NP-templated supraparticles, whilst in ζ-potential measurements we detected a decrease to 20 ± 5 mV in comparison to chitosan particles solely loaded with nanodiamonds. Fig. S5 (ESI†) provides additional TEM micrographs comparing the native, ND loaded, as well as ND loaded and S–SiO$_2$-NP templated supraparticles. Also, as indicated above, after the dialysis step, the majority of the supraparticle dispersion was transferred to a new vial for storage and the dispersion, as well as the other samples, showed no signs of agglomeration
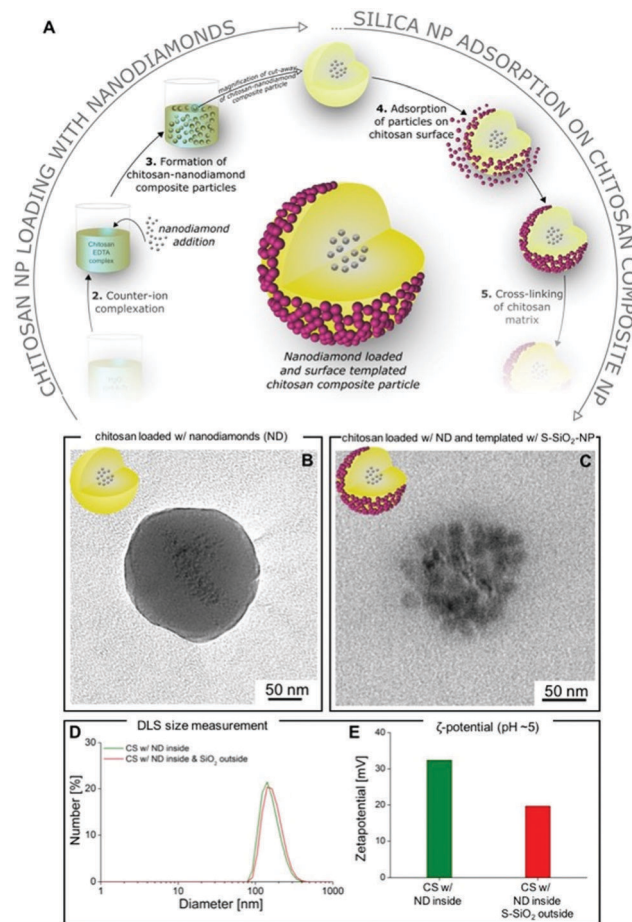
or sediment formation afterwards (see Fig. S6 for photographs of the different dispersions, ESI†). In conclusion, this synthesis route represents a novel way for the controlled synthesis of nanoparticle core-loaded and surface-templated nano-scaled supraparticles with distinct functionality.

Conclusions and outlook

In summary, we have presented a new type of chitosan-based supraparticle synthesis route with tailor-made nanoparticle surface templating and/or core-loading. The synthesis route, performed at a mild pH, allows for a unique core–shell architecture and the utilized nanoparticle types may be easily exchanged for other functional colloids like iron oxide or gold nanoparticles in future studies. Miniaturization of multivalent particles and capsules towards sizes significantly below 1 micrometer plays a pivotal role in their potential implementation in chemical and materials engineering as well as bionanotechnology applications. Various challenges still remain, including the further functionalization of the surface of the chitosan complexes with biocompatibility

enhancing molecules like zwitter ions or poly(ethylene glycol) for enhanced stealth capabilities. Also, a further decrease in size to approx. 50 nm is desired, to potentially inhibit accumulation within the mononuclear phagocyte system and to passively target tumors by utilizing the enhanced permeability and retention effect. Furthermore, cross-linking of the chitosan particles with *e.g.* genipin could also increase their intrinsic biocompatibility and tailor their biodegradation behaviour.[55] Overall, the architecture of the structures renders them of high interest for bionanotechnology applications and the supraparticles synthesis represent a versatile platform for the design of potentially biocompatible and multifunctional nanoprobes in future studies.

Acknowledgements

References

1 X.-C. Yang, B. Samanta, S. S. Agasti, Y. Jeong, Z.-J. Zhu, S. Rana, O. R. Miranda and V. M. Rotello, *Angew. Chem., Int. Ed.*, 2011, **50**, 477–481.

2 O. Chen, L. Riedemann, F. Etoc, H. Herrmann, M. Coppey, M. Barch, C. T. Farrar, J. Zhao, O. T. Bruns, H. Wei, P. Guo, J. Cui, R. Jensen, Y. Chen, D. K. Harris, J. M. Cordero, Z. Wang, A. Jasanoff, D. Fukumura, R. Reimer, M. Dahan, R. K. Jain and M. G. Bawendi, *Nat. Commun.*, 2014, **5**, 5093.

3 C. Wu, S. Bai, M. B. Ansorge-Schumacher and D. Wang, *Adv. Mater.*, 2011, **23**, 5694–5699.

4 A.-M. Cao, J.-S. Hu, H.-P. Liang and L.-J. Wan, *Angew. Chem., Int. Ed.*, 2005, **44**, 4391–4395.

5 N. Vogel, S. Utech, G. T. England, T. Shirman, K. R. Phillips, N. Koay, I. B. Burgess, M. Kolle, D. A. Weitz and J. Aizenberg, *Proc. Natl. Acad. Sci. U. S. A.*, 2015, **112**, 10845–10850.

6 Z. Lu and Y. Yin, *Chem. Soc. Rev.*, 2012, **41**, 6874–6887.

7 J. K. Stolarczyk, A. Deak and D. F. Brougham, *Adv. Mater.*, 2016, **28**, 5400–5424.

8 O. D. Velev, K. Furusawa and K. Nagayama, *Langmuir*, 1996, **12**, 2374–2384.

9 A. D. Dinsmore, M. F. Hsu, M. G. Nikolaides, M. Marquez, A. R. Bausch and D. A. Weitz, *Science*, 2002, **298**, 1006–1009.

10 E. R. Zubarev, J. Xu, A. Sayyad and J. D. Gibson, *J. Am. Chem. Soc.*, 2006, **128**, 15098–15099.

11 Z. Nie, D. Fava, E. Kumacheva, S. Zou, G. C. Walker and M. Rubinstein, *Nat. Mater.*, 2007, **6**, 609–614.

12 F. Caruso, R. A. Caruso and H. Möhwald, *Science*, 1998, **282**, 1111–1114.

13 M. S. Fleming, T. K. Mandal and D. R. Walt, *Chem. Mater.*, 2001, **13**, 2210–2216.

14 T. Bollhorst, K. Rezwan and M. Maas, *Chem. Soc. Rev.*, 2017, in press.

15 T. Bollhorst, T. Grieb, A. Rosenauer, G. Fuller, M. Maas and K. Rezwan, *Chem. Mater.*, 2013, **25**, 3464–3471.

16 Y. Liu, J.-J. Yin and Z. Nie, *Nano Res.*, 2014, **7**, 1719–1730.

17 T. Yokoi, Y. Sakamoto, O. Terasaki, Y. Kubota, T. Okubo and T. Tatsumi, *J. Am. Chem. Soc.*, 2006, **128**, 13664–13665.

18 M. A. Snyder, J. A. Lee, T. M. Davis, L. E. Scriven and M. Tsapatsis, *Langmuir*, 2007, **23**, 9924–9928.

19 K. Zarschler, L. Rocks, N. Licciardello, L. Boselli, E. Polo, K. P. Garcia, L. De Cola, H. Stephan and K. A. Dawson, *Nanomedicine*, 2016, **12**, 1663–1701.

20 E. Phillips, O. Penate-Medina, P. B. Zanzonico, R. D. Carvajal, P. Mohan, Y. Ye, J. Humm, M. Gönen, H. Kalaigian, H. Schöder, H. W. Strauss, S. M. Larson, U. Wiesner and M. S. Bradbury, *Sci. Transl. Med.*, 2014, **6**, 260ra149.

21 S. E. Kim, L. Zhang, K. Ma, M. Riegman, F. Chen, I. Ingold, M. Conrad, M. Z. Turker, M. Gao, X. Jiang, S. Monette, M. Pauliah, M. Gonen, P. Zanzonico, T. Quinn, U. Wiesner, M. S. Bradbury and M. Overholtzer, *Nat. Nanotechnol.*, 2016, **11**, 977–985.

22 M. Yu and J. Zheng, *ACS Nano*, 2015, **9**, 6655–6674.

23 Y. Lin, H. Skaff, T. Emrick, A. D. Dinsmore and T. P. Russell, *Science*, 2003, **299**, 226–229.

24 A. Schrade, Z. Cao, K. Landfester and U. Ziener, *Langmuir*, 2011, **27**, 6689–6700.

25 K. L. Thompson, M. Williams and S. P. Armes, *J. Colloid Interface Sci.*, 2015, **447**, 217–228.

26 J.-W. Kim, A. Fernández-Nieves, N. Dan, A. S. Utada, M. Marquez and D. A. Weitz, *Nano Lett.*, 2007, **7**, 2876–2880.

27 M. Karg, I. Pastoriza-Santos, J. Pérez-Juste, T. Hellweg and L. M. Liz-Marzán, *Small*, 2007, **3**, 1222–1229.

28 M. Karg, Y. Lu, E. Carbó-Argibay, I. Pastoriza-Santos, J. Pérez-Juste, L. M. Liz-Marzán and T. Hellweg, *Langmuir*, 2009, **25**, 3163–3167.

29 K. Gawlitza, S. T. Turner, F. Polzer, S. Wellert, M. Karg, P. Mulvaney and R. von Klitzing, *Phys. Chem. Chem. Phys.*, 2013, **15**, 15623.

30 B. Du, Z. Cao, Z. Li, A. Mei, X. Zhang, J. Nie, J. Xu and Z. Fan, *Langmuir*, 2009, **25**, 12367–12373.

31 M. Chen, L. Wu, S. Zhou and B. You, *Macromolecules*, 2004, **37**, 9613–9619.

32 M. Chen, S. Zhou, B. You and L. Wu, *Macromolecules*, 2005, **38**, 6411–6417.

33 M. Destribats, V. Schmitt and R. Backov, *Langmuir*, 2010, **26**, 1734–1742.

34 M. Depardieu, M. Nollet, M. Destribats, V. Schmitt and R. Backov, *Part. Part. Syst. Charact.*, 2013, **30**, 185–192.

35 R. T. Rosenberg and N. Dan, *J. Biomater. Nanobiotechnol.*, 2011, **02**, 1–7.

36 M. A. Cooperstein and H. E. Canavan, *Biointerphases*, 2013, **8**, DOI: 10.1186/1559-4106-8-19.

37 N. Kamaly, B. Yameen, J. Wu and O. C. Farokhzad, *Chem. Rev.*, 2016, **116**, 2602–2663.

38 J. Kumirska, M. X. Weinhold, J. Thöming and P. Stepnowski, *Polymers*, 2011, **3**, 1875–1901.

39 Q. Gan and T. Wang, *Colloids Surf., B*, 2007, **59**, 24–34.

40 H.-W. Sung, K. Sonaje, Z.-X. Liao, L.-W. Hsu and E.-Y. Chuang, *Acc. Chem. Res.*, 2012, **45**, 619–629.

41 A. M. Dyer, M. Hinchcliffe, P. Watts, J. Castile, I. Jabbal-Gill, R. Nankervis, A. Smith and L. Illum, *Pharm. Res.*, 2002, **19**, 998–1008.

42 H. Du, X. Yang and G. Zhai, *Nanomedicine*, 2014, **9**, 723–740.

43 L. Hu, Y. Sun and Y. Wu, *Nanoscale*, 2013, **5**, 3103–3111.

44 Y. Luo and Q. Wang, *Int. J. Biol. Macromol.*, 2014, **64**, 353–367.

45 M.-C. Chen, F.-L. Mi, Z.-X. Liao, C.-W. Hsiao, K. Sonaje, M.-F. Chung, L.-W. Hsu and H.-W. Sung, *Adv. Drug Delivery Rev.*, 2013, **65**, 865–879.

46 H. Ragelle, G. Vandermeulen and V. Préat, *J. Controlled Release*, 2013, **172**, 207–218.

47 S. M. Lim, D. K. Song, S. H. Oh, D. S. Lee-Yoon, E. H. Bae and J. H. Lee, *J. Biomater. Sci., Polym. Ed.*, 2008, **19**, 453–466.

48 R. Guo, L. Zhang, Z. Zhu and X. Jiang, *Langmuir*, 2008, **24**, 3459–3464.

49 R. Guo, L. Zhang, H. Qian, R. Li, X. Jiang and B. Liu, *Langmuir*, 2010, **26**, 5428–5434.

50 C. A. S. Batista, R. G. Larson and N. A. Kotov, *Science*, 2015, **350**, 1242477.

51 S. Shahabi, L. Treccani and K. Rezwan, *J. Nanopart. Res.*, 2015, **17**, 1–15.

52 K. Ma, C. Mendoza, M. Hanson, U. Werner-Zwanziger, J. Zwanziger and U. Wiesner, *Chem. Mater.*, 2015, **27**, 4119–4133.

53 K. Ma, D. Zhang, Y. Cong and U. Wiesner, *Chem. Mater.*, 2016, **28**, 1537–1545.

54 M. Maas, T. Bollhorst, R. N. Zare and K. Rezwan, *Part. Part. Syst. Charact.*, 2014, **31**, 1067–1071.

55 M. Arteche Pujana, L. Pérez-Álvarez, L. C. Cesteros Iturbe and I. Katime, *Carbohydr. Polym.*, 2013, **94**, 836–842.

56 M. X. Weinhold, J. C. M. Sauvageau, J. Kumirska and J. Thöming, *Carbohydr. Polym.*, 2009, **78**, 678–684.

57 S. Lu, X. Song, D. Cao, Y. Chen and K. Yao, *J. Appl. Polym. Sci.*, 2004, **91**, 3497–3503.

58 T. G. Mason, J. N. Wilking, K. Meleson, C. B. Chang and S. M. Graves, *J. Phys.: Condens. Matter*, 2006, **18**, R635.

59 F. Caruso, *Adv. Mater.*, 2001, **13**, 11–22.

60 Q. Tian, S. Liu, X. Sun, H. Sun, Z. Xue and T. Mu, *Carbohydr. Res.*, 2015, **408**, 107–113.

61 M. Rinaudo, G. Pavlov and J. Desbrières, *Polymer*, 1999, **40**, 7029–7032.

62 P. Dušak, A. Mertelj, S. Kralj and D. Makovec, *J. Colloid Interface Sci.*, 2015, **438**, 235–243.

63 T. Bollhorst, S. Shahabi, K. Wörz, C. Petters, R. Dringen, M. Maas and K. Rezwan, *Angew. Chem., Int. Ed.*, 2015, **54**, 118–123.

64 E. Herz, A. Burns, S. Lee, P. Sengupta, D. Bonner, H. Ow, C. Liddell, B. Baird and U. Wiesner, *Proc. SPIE*, 2006, **6096**, 609605.

65 J. Song, X. Yang, O. Jacobson, L. Lin, P. Huang, G. Niu, Q. Ma and X. Chen, *ACS Nano*, 2015, **9**, 9199–9209.

66 R. E. Serda, B. Godin, E. Blanco, C. Chiappini and M. Ferrari, *Biochim. Biophys. Acta, Gen. Subj.*, 2011, **1810**, 317–329.